Original Article

Quantification of pancreatic iron overload and fat infiltration and their correlation with glucose disturbance in pediatric thalassemia major patients

Jingwen Huang[1#], Jun Shen[1#], Qihua Yang[1], Ziliang Cheng[1], Xiaodong Chen[2], Taihui Yu[1], Jinglian Zhong[1], Yun Su[1], Hua Guo[3], Biling Liang[1]

[1]Department of Radiology, Sun Yat-sen Memorial Hospital, Sun Yat-sen University, Guangzhou, China; [2]Department of Radiology, Affiliated hospital of Guangdong Medical University, Zhanjiang, China; [3]Center for Biomedical Imaging Research, Department of Biomedical Engineering, Tsinghua University, Beijing, China

[#]These authors contributed equally to this work.

Correspondence to: Biling Liang. Department of Radiology, Sun Yat-sen Memorial Hospital, Sun Yat-sen University, No. 107 Yanjiang Road West, Guangzhou 510120, China. Email: liangbl@163.net; Hua Guo. Center for Biomedical Imaging Research, Department of Biomedical Engineering, Tsinghua University, No. 30 Shuangqing Road, Beijing 100084, China. Email: huaguo@tsinghua.edu.cn.

Background: Diabetes mellitus affects more than a quarter of patients with thalassemia major (TM) worldwide, and increases the risk for cardiac complications, contributing to significant morbidity. Pancreatic iron overload (IO) and fat infiltration have been correlated with this endocrinal complication in adult TM patients. It has been shown that in adult TM patients, iron accumulation and fat infiltration are found to be heterogeneous in the pancreatic head, body, and tail region. R2* and a fat fraction (FF) generated by gradient-echo imaging can be used as quantitative parameters to assess the iron and fat contents of the pancreas. This study aimed to determine the pattern of pancreatic iron accumulation and fat infiltration in pediatric TM patients with gradient-echo imaging and evaluate the association between pancreatic IO and fat infiltration and glucose disturbances.

Methods: A total of 90 children with TM (10.7±3.1 years) were included. All patients underwent pancreatic magnetic resonance imaging (MRI) using multi-echo gradient-echo sequences. IO was measured by R2* relaxometry in 90 patients, and FF values were measured using iterative decomposition of water and fat with echo asymmetry and the least-squares estimation (IDEAL) method in 40 patients. R2* and FF were assessed in the pancreatic head, body, and tail. The global R2* and global FF values were obtained by averaging the respective values from the pancreatic head, body, and tail. The correlations between global R2*, global FF, and fasting glucose were determined using Spearman's correlation analysis. The Friedman test was used to compare R2* and FF among different pancreatic regions. Receiver operating characteristic (ROC) analysis was used to determine the performance of global R2* and global FF in discriminating impaired fasting glucose from normal fasting glucose patients.

Results: The global R2* was positively correlated with the global FF in the pancreas (r=0.895, P<0.001). No significant differences were found in R2* among the 3 regions of the pancreas (χ^2=4.050, P=0.132), but significant differences were found in FF among the 3 pancreatic regions (χ^2=16.350, P<0.001). Both global pancreatic R2* (r=0.408, P<0.001) and global FF (r=0.523, P=0.001) were positively correlated with fasting glucose. ROC analysis showed that global pancreatic R2* and global FF had an area under the curve of 0.769 and 0.931 (both P<0.001), respectively, in discriminating between impaired and normal glucose function patients.

Conclusions: Pediatric TM patients can have homogeneous iron siderosis and heterogeneous fat infiltration in the pancreas as measured by gradient-echo imaging, both of which are risk factors for diabetes.

Keywords: Fat infiltration; iron overload (IO); magnetic resonance imaging (MRI); pancreas; thalassemia

Submitted Feb 17, 2020. Accepted for publication Sep 25, 2020.
doi: 10.21037/qims-20-292
View this article at: http://dx.doi.org/10.21037/qims-20-292

Introduction

Transfusion-related iron overload (IO) is common in patients with thalassemia major (TM) (1). It is known that pancreatic IO can induce endocrinal complications such as diabetes mellitus (DM) (2,3), which might be caused by insulin deficiency resulting from the direct toxic effect of excess iron in pancreatic beta cells (4). This endocrinal complication is reported to affect 6.4–26.8% of TM patients worldwide (1,5), and increases the risk of cardiac complications, such as heart failure, hyperkinetic arrhythmias, and myocardial fibrosis, contributing to significant morbidity in TM patients (1,6,7). Early application of chelation therapy is protective for DM induced by pancreatic IO (8). Moreover, pancreatic IO may be an alternative predictor of cardiac IO in TM patients (9,10). Thus, detection and monitoring of pancreatic iron accumulation are necessary for the effective prevention and treatment of potential DM in TM patients, and even for effective prevention of cardiac complications in the long term. Conventionally, iron burden assessment is based on the serum ferritin test. Besides serum ferritin, the evaluation of body IO by non-invasive magnetic resonance imaging (MRI) using R2- (T2) or R2*- (T2*) relaxometry has been established clinically in recent years (11). It has been reported that MRI can reliably measure hepatic (12,13), cardiac (14,15), and pancreatic iron concentration (3) in TM patients. It has also been shown that in adult TM patients, iron accumulation is found to be heterogeneous in the pancreatic head, body, and tail region (16). However, whether iron is heterogeneously accumulated in different pancreatic regions in pediatric TM patients remains unknown.

In addition to iron accumulation, fat infiltration of the pancreas has been previously reported in adult TM patients with IO (16,17). This fatty replacement of the pancreas is commonly seen in adult TM patients with overt DM (17), resulting from the progressive replacement of pancreatic parenchyma by inert adipose tissue after pancreatic cells die from the cytotoxic effects of iron (18,19). However, there is little data on pancreatic fat infiltration in pediatric TM patients. Only 3 teenage TM patients have been reported with elevated fat fraction (FF) levels in the pancreas (20). Pancreatic fat infiltration in pediatric TM patients and its association with glucose disturbances remains to be assessed.

In this study, non-invasive MRI was performed in pediatric TM patients to quantitatively measure pancreatic IO and fat infiltration. The purpose of this study was to determine the pattern of pancreatic iron accumulation and fat infiltration in pediatric TM patients and to evaluate the association between pancreatic IO and fat infiltration, and glucose disturbances.

Methods

Patients

Between May 2015 and January 2016, 99 consecutive outpatient children with TM were enrolled. The institutional review board approved this prospective study of Sun Yat-sen Memorial Hospital of Sun Yat-sen University (No: 2013-19). Written informed consent was obtained from all patients or their parents. All patients were diagnosed with TM by genetic analysis. Patients were excluded if they were overweight, defined by body mass index (BMI) exceeding the normal reference line (21), or had a family history of diabetes. Two overweight patients and 1 patient with a family history of diabetes were excluded. Additionally, 6 patients with obvious motion artifacts on MRI were also excluded. Finally, 90 children (mean age, 10.7±3.1 years; age range 5.0–17.5 years) consisting of 64 boys (mean age, 10.5±3.1 years; age range 5.0–17.0 years) and 26 girls (mean age, 11.3±3.0 years; age range 6.0–17.5 years) were included in this study.

MRI protocol

All patients underwent pancreatic MRI. Pancreatic R2* relaxometry was performed on a 1.5 T MR scanner (Intera, Philips Medical Systems, Best, The Netherlands) with a 4-channel SENSE body coil. Pancreatic FF measurement was performed on a 3.0 T MR scanner (Achieva, Philips Medical Systems, Best, The Netherlands) with a 16-channel SENSE torso coil. All patients underwent pancreatic R2* measurements, and 40 of them underwent FF measurements randomly. For pancreatic R2* relaxometry, 16-echo gradient-echo imaging was performed to measure

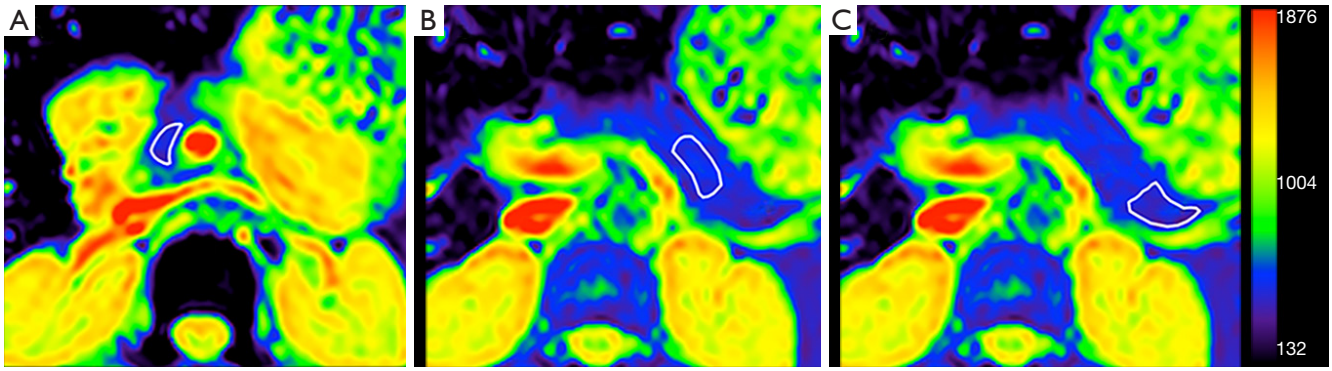

Figure 1 Axial pseudo-colorized images derived from T2* relaxometry scans in a 13-year-old female patient with thalassemia major. Three different free-hand ROIs of 1–2 cm^2 were manually placed in the pancreas head (A), body (B), and tail (C), with a sufficient distance maintained from gland boundaries and vascular structures. ROI, region of interest.

T2* values. This sequence was performed with the additional application of chemically selective fat suppression (CHESS), which takes advantage of the difference in resonant frequencies between water and fat. The detailed acquisition parameters were as follows: 2D acquisition, no SENSE, voxel size 2.5×3.1×10 mm^3, field-of-view (FOV) 400×200 mm^2, repetition time (TR) 200 ms, echo times (TE) ranging from 0.84 to 14.69 ms, ΔTE =0.92 ms, flip angle 20°, single breath-hold of 16 seconds, number of slices 3, set separately on the pancreatic head, body, and tail level. For pancreatic FF, 6-echo gradient-echo imaging was performed. The detailed acquisition parameters were as follows: 2D acquisition, no SENSE, voxel size 1.8×1.8×8.0 mm^3, FOV 290×188 mm^2, TR 16 ms, TE ranging from 1.4 to 3.9 ms, ΔTE =0.5 ms, flip angle 10°, single breath-hold of 12 seconds, number of slices 3, set separately on the pancreatic head, body, and tail level.

Image analysis

T2* values were computed using Thalassemia tools (a plugin of CMRtools, Cardiovascular Imaging Solutions, 2012 version, London, UK). The value of T2* relaxation time was derived with an equation of $y=Ke^{-TE/T2^*}$, where K represents a constant, TE represents echo times, and y represents the image signal intensity (15). A truncation model was used to correct the bias caused by background noise at long TEs and improve the curve fit (22). The fitting quality of T2* measurements obtained by CMRtools was recorded. FF maps were calculated using the iterative decomposition of water and fat with echo asymmetry and least-squares estimation (IDEAL) algorithm (23). Region of interests (ROI) were drawn on the FF maps using image J software (NIH, Bethesda, MD) to measure the FF values. For both T2* and FF measurements, an ROI of 1–2 cm^2 was manually placed on the pancreas head, body, and tail, respectively (*Figure 1*), as previously described (16). Only clearly identified and demarcated pancreatic tissue was considered for analysis. ROIs were drawn by 2 radiologists independently (with 5 years and 3 years of experience with abdominal MRI). The global R2* and global FF values were obtained by averaging the respective values from the pancreatic head, body, and tail. The T2* relaxation time was transformed into reciprocal R2* according to the following formula: R2* (s^{-1}) = 1,000/T2* (ms). A global pancreatic R2* value <30 s^{-1} was considered normal, 30 s^{-1} <R2*<100 s^{-1} was considered mild IO, 100 s^{-1} <R2*<400 s^{-1} was considered moderate IO, and R2*>400 s^{-1} was considered severe IO (24). FF>0.065 was considered abnormal (25).

Laboratory tests

Laboratory tests were performed using blood samples collected within 1 week before or after the MRI examination. All 90 patients underwent serum ferritin, fasting blood glucose (FBG), and fasting insulin tests. According to the American Diabetes Association criteria (26), patients were classified with normal glucose function if they had FBG <5.6 mmol/L; impaired fasting glucose (IFG) if FBG was between 5.6–6.9 mmol/L, and DM if FBG >7.0 mmol/L. The homeostasis model assessment (HOMA) indexes were also calculated according to the following formulae: HOMA-β (beta cell function) (normal range: 130–400%) = insulin ×20/glucose-3.5 and HOMA-

Table 1 Demographics of the 90 pediatric patients with thalassemia major.

	Group A[†] (n=74)	Group B[‡] (n=16)	Z or χ^2 value	P value
Age (years)	10.29±2.82	12.63±3.50	2.494	0.013
Gender, male/female	53/21 (72%:28%)	11/5 (69%:31%)	0.053[§]	0.818
BMI, kg/m^2	15.71±1.74	16.87±1.45	2.764	0.006
Initial transfusion time (months)	20.39±21.59	15.69±17.07	0.883	0.377
Transfusion duration (years)	8.27±2.84	10.97±4.05	2.765	0.006
Total blood input (L)	59.30±35.52	67.51±33.43	1.551	0.121
Initial chelation time (years)	4.72±2.72	4.97±2.98	0.345	0.730
Chelation duration (years)	5.34±2.97	7.59±4.44	1.594	0.111
SF (μg/L)	3401±1988	3580±2224	0.227	0.820
Fasting insulin (mU/L)	6.24±3.58	6.98±2.52	1.422	0.155
HOMA-β (%)	95.29±64.37	56.89±21.44	1.769	0.770
HOMA-IR	1.37±0.79	1.86±0.67	2.042	0.041

The continuous variables are reported as mean ± SD, and categorical variables are reported as frequencies with percentage in parentheses. [†]Group A, patients with normal glucose function; [‡]Group B, patients with impaired glucose function. [§]χ^2 value. SD, standard deviation; BMI, body mass index; SF, serum ferritin; FBG, fasting blood glucose; HOMA, homeostasis model assessment; IR, insulin resistance.

IR (insulin resistance) (normal range: 0.8–1.6) =insulin × glucose/22.5 (2).

Statistical analysis

Agreement in MRI evaluation between the 2 readers was calculated using the intraclass correlation coefficient (ICC). An ICC value >0.75 represented good to excellent agreement. Data from the 2 readers was averaged for analysis. The global R2*, global FF, and clinical parameters between patients with elevated and normal fasting glucose were compared using the Mann-Whitney U test or Chi-square test. Box and whisker plots were used to display the differences in the global pancreatic R2* and FF in patients with normoglycemia versus patients with IFG. The Friedman test was used to compare R2* and FF among the 3 different regions of the pancreas, and differences between subgroups were determined using the paired Wilcoxon-Mann-Whitney test. Scatter plots were generated to show the correlations in R2* and FF among the 3 pancreatic regions. Linear regression analysis was performed to further test the relationship of R2* among the 3 different pancreas regions in patients with mild to moderate pancreatic IO. Correlations among the biochemical parameters, global R2*, and global FF were determined using Spearman's correlation analysis. Receiver operating characteristic (ROC) analysis was used to determine the performance of global pancreatic R2* and global FF for discrimination between patients with normal and impaired glucose function. The Youden index determined the optimal threshold. All statistical analysis was performed in SPSS (version 13.0, SPSS Inc., Chicago, IL). A two-sided P value of less than 0.05 was considered statistically significant.

Results

Patient demographics

The demographic data for all patients are summarized in *Table 1*. Patients were assigned to 2 groups according to FBG levels. A total of 74 out of 90 (82.2%) patients who had normal glucose function were assigned to group A, and the remaining 16 (17.8%) patients who had IFG were assigned to group B. None of the patients had DM. A total of 72 out of 90 (80%) patients had low HOMA-β levels, and 36 of 90 (40%) patients had high HOMA-IR levels. Significant differences were found in age, BMI, transfusion duration, and HOMA-IR between the 2 groups (*Table 1*). Patients with IFG were older, had a higher BMI, and were in a more severe insulin resistance state, compared to those

Table 2 Agreements in R2* and FF evaluation between the 2 readers

	Pancreatic head (95% CI)	Pancreatic body (95% CI)	Pancreatic tail (95% CI)	Global (95% CI)
ICC for R2*	0.994 (0.991–0.996)	0.987 (0.981–0.991)	0.983 (0.975–0.989)	0.998 (0.993–0.997)
ICC for FF	0.926 (0.864–0.960)	0.914 (0.844-0.954)	0.838 (0.714–0.911)	0.984 (0.943–0.984)

FF, fat fraction; ICC, intraclass correlation coefficient; CI, confidence interval.

Table 3 The R2* and FF values across the 3 regions of the pancreas.

	Pancreatic head	Pancreatic body	Pancreatic tail	χ^2	P value
R2*(s^{-1})†	189.50±158.30	189.34±146.19	194.64±156.91	4.050	0.132
FF‡	0.12±0.11	0.12±0.09	0.13±0.10	16.350	<0.001

R2* and FF values are reported as mean ± SD. †90 patients; ‡40 patients. FF, fat fraction; SD, standard deviation.

with normoglycemia.

R2 and FF*

For the T2* measurement, the fitting quality obtained by CMR tools was 0.994±0.004. For the R2* and FF evaluation, the agreements between the 2 readers are shown in *Table 2*. The R2* and FF values in the pancreatic head, body, and tail are shown in *Table 3*. No significant differences were found in R2* among the 3 pancreatic regions (χ^2=4.050, P=0.132). However, significant differences were found in FF among the 3 pancreatic regions (χ^2=16.350, P<0.001). Further comparisons between subgroups showed that pancreatic FF was similar between the head and body (Z=1.425, P=0.154), but FF in the tail was significantly higher than in the head (Z=3.663, P<0.001) and the body (Z=2.057, P=0.04). The scatter plots (*Figure 2*) showed that significant correlations were found in R2* between the pancreatic head, body, and tail (r=0.930, 0.962, 0.967; all P<0.001), along with significant correlations in FF between the pancreatic head, body, and tail (r=0.876, 0.810, 0.913; all P<0.001). Linear regression analysis showed a positive linear correlation in R2* among the 3 different regions (R-squared=0.919, 0.869, 0.927; all P<0.001) in patients with mild to moderate IO. The slopes were 0.942 (95% CI: 0.879–1.005), 0.945 (95% CI: 0.862–1.027), and 0.992 (95% CI: 0.930–1.055) for head-body, head-tail, and body-tail, respectively. In the 90 patients who underwent R2* relaxometry, 96.7% (87/90) of patients had detectable pancreatic IO, 30.0% (27/90) of patients had mild pancreatic IO, 55.6% (50/90) of patients had moderate pancreatic IO, and 11.1% (10/90) of patients had severe pancreatic IO. In the 40 patients who underwent pancreatic FF measurement calculated using the IDEAL algorithm, 60% (24/40) of patients had elevated global FF levels. The youngest patient with elevated global FF levels was 6 years old. In the 40 patients who underwent both R2* relaxometry and FF measurements, the global pancreatic FF was positively correlated with the global R2* (r=0.895, P<0.001, *Figure 3*). A total of 38 out of 40 patients had pancreatic IO. Among the 38 patients with pancreatic IO, 24 (63%) patients had elevated global FF levels.

Association between the global pancreatic R2, global FF, and glucose metabolism*

FBG was positively correlated with the global pancreatic R2* (r=0.408, P<0.001) (*Figure 4A*) and the global FF (r=0.523, P=0.001) (*Figure 4B*). The global pancreatic R2* and FF were significantly different between patients with IFG and those with normoglycemia (*Z*=3.356, 3.333, respectively, both P=0.001) (*Table 4*). The global R2* and FF values were higher in patients with IFG than those with normoglycemia (*Figure 5*).

ROC curves were calculated (*Figure 6*) for the global pancreatic R2* and FF to discriminate patients with IFG from those with normal glucose function. The global pancreatic FF demonstrated good discriminatory power, with an area under the curve (AUC) of 0.931 (95% CI: 0.851–1.011), and a sensitivity of 83.3% and specificity of 88.2% at a cut-off level of 0.18 (P<0.001). The global pancreatic R2* demonstrated medium discriminatory power, with an AUC of 0.769 (95% CI: 0.610–0.927), and a sensitivity of 75.0% and specificity of 75.7% at a cut-off level of 215 s^{-1} (P<0.001).

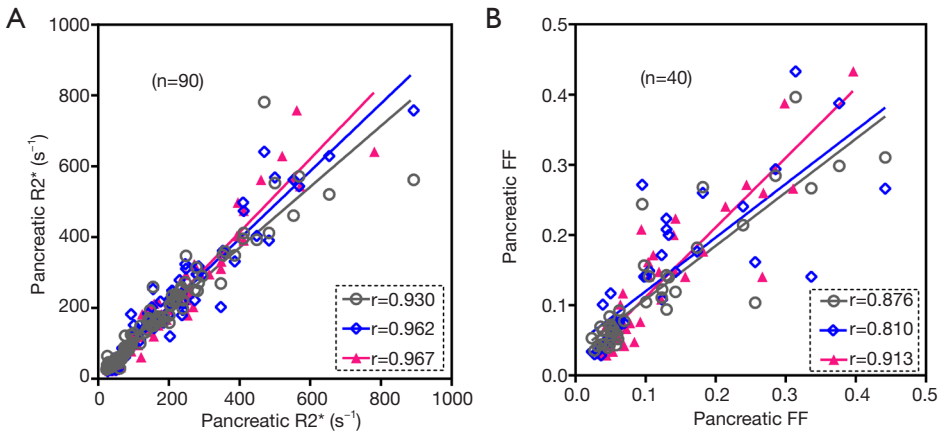

Figure 2 Scatter plots of R2* and FF across the 3 different regions of the pancreas. (A) Correlations in R2* values across different regions of the pancreas. Significant correlations were found in R2* values, with a correlation coefficient of 0.930 between the pancreatic head and body (grey ring), 0.962 between the pancreatic head and tail (dark blue diamond), and 0.967 between the pancreatic body and tail (rose red triangle), all with P<0.001. (B) Correlations in FF values across different regions of the pancreas. Significant correlations were found in FF values, with a correlation coefficient of 0.876 between the pancreatic head and body (grey ring), 0.810 between the pancreatic head and tail (dark blue diamond), and 0.913 between the pancreatic body and tail (rose red triangle), all with P<0.001. FF, fat fraction.

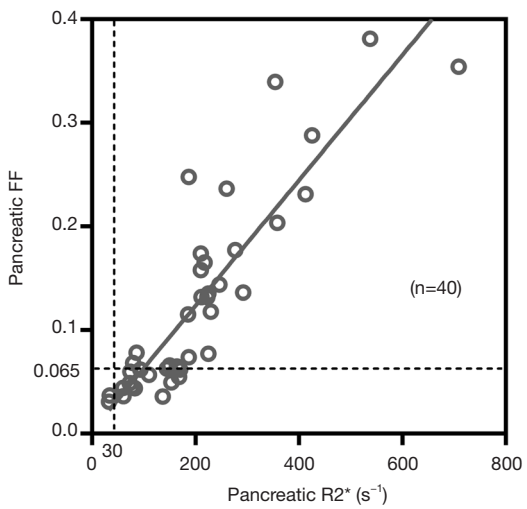

Figure 3 Scatter plot of the global pancreatic R2* and FF. The graph shows that the global pancreatic FF was positively correlated with the global R2* (r=0.895, P<0.001). The vertical dashed line represents the cut point of abnormal pancreatic R2* values. The horizontal dashed line represents the cut point of the elevated FF level. FF, fat fraction.

Discussion

Our study showed that in pediatric TM patients, iron deposition in the pancreatic head, body, and tail showed a trend from relatively homogenous distribution to heterogeneous distribution as IO increased. Fatty replacement in the pancreas was heterogeneously distributed among the 3 different pancreatic regions. Furthermore, pancreatic fatty replacement correlated with pancreatic IO. Both pancreatic iron accumulation and fatty replacement as measured by gradient-echo imaging were associated with fasting glucose, and demonstrated an effective ability to discriminate between patients with impaired glucose function and normoglycemia.

Pancreatic iron loading begins in early childhood in TM patients (1,10,27). Excessive iron has a direct toxic effect on pancreatic beta cells causing cell death, which results in insulin deficiency and leads to the development of DM in TM patients (4). When pancreatic cells die from the cytotoxic effects of iron, the pancreatic parenchyma is progressively replaced by inert adipose tissue (18,19). Clinically, the serum ferritin test is routinely applied to measure and monitor iron stores. However, this method is not always reliable because inflammation and liver damage can also increase serum ferritin levels (28). Moreover, the serum ferritin test can reflect total body iron burden but not the precise iron overload among different solid organs. MRI R2* relaxometry can overcome this limitation, and has thus emerged as the dominant non-invasive modality for tissue iron quantification in clinical practice (11). It has been shown that MRI can reliably measure iron deposition in the heart, liver, and pancreas accurately via T2* relaxation

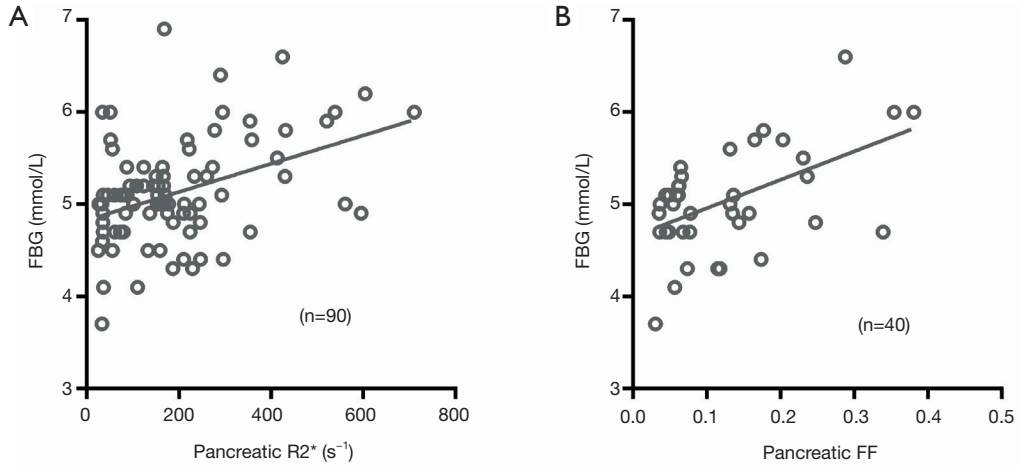

Figure 4 Scatter plots of the global pancreatic R2*, FF, and FBG. The FBG was positively correlated with the (A) global pancreatic R2* (r=0.408, P<0.001) and (B) FF (r=0.523, P=0.001). FF, fat fraction. FBG, fasting blood glucose.

Table 4 Comparison between pancreatic R2* and FF between groups with normal and impaired glucose function

	Group A[†]	Group B[‡]	Z value	P value
Pancreatic R2* (s^{-1})[§]	157.80±115.42 (n=74)	333.13±201.29 (n=16)	3.356	0.001
Pancreatic FF[¶]	0.10±0.07 (n=34)	0.21±0.06 (n=6)	3.333	0.001

[†]Group A, patients with normal glucose function; [‡]Group B, patients with impaired fasting glucose; [§]90 patients; [¶]40 patients. FF, fat fraction.

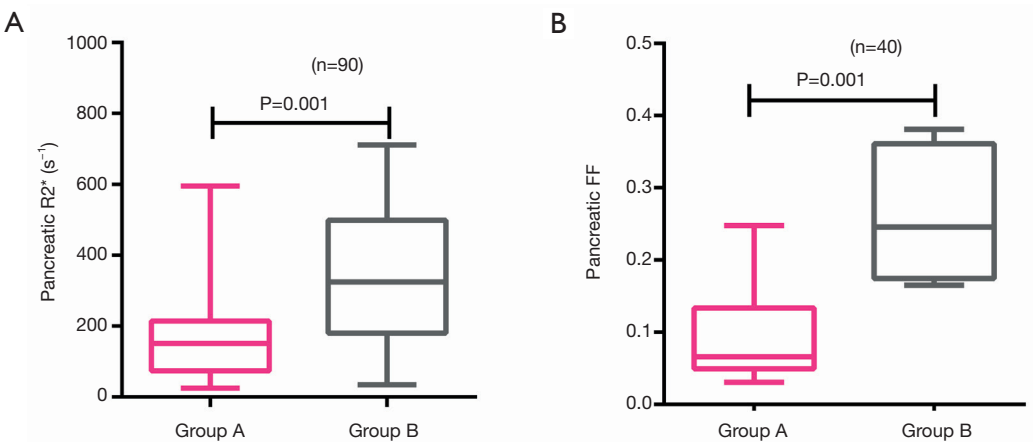

Figure 5 Box and whisker plots of the global pancreatic R2* (A) and FF (B) in group A (patients with normoglycemia) versus group B (patients with IFG). Patients with IFG had higher global R2* and FF levels, compared to patients with normoglycemia (both P=0.001). FF, fat fraction. IFG, impaired fasting glucose.

time measurement (3,13,15), and pancreatic R2* (1/T2*) is the strongest predictor of beta cell function in TM (3). The IDEAL algorithm has been widely used to calculate fat content in multiple regions of the body, including the pancreas on 1.5T and 3.0T MR scanners (20,23,29-31). It has been reported that fatty replacement of the pancreas

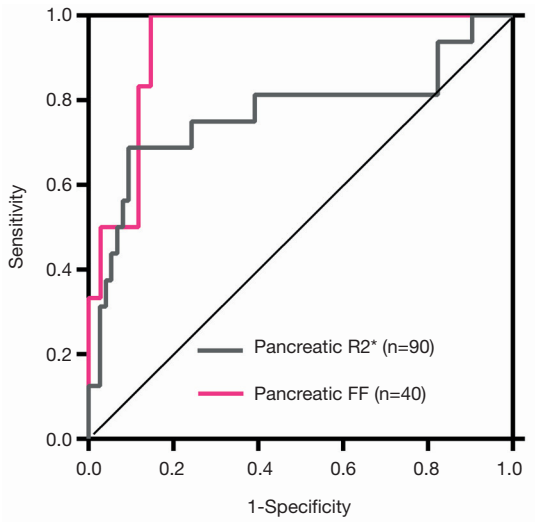

Figure 6 ROC curves of the global pancreatic R2* (grey curve) and the global pancreatic FF (rose red curve) to discriminate between patients with IFG versus those with normoglycemia. The global pancreatic FF demonstrated good discriminatory power with an AUC of 0.931 (95% CI: 0.851–1.011) (P<0.001). The global pancreatic R2* demonstrated medium discriminatory power with an AUC of 0.769 (95% CI: 0.610–0.927) (P<0.001). FF, fat fraction. IFG, impaired fasting glucose. AUC, area under the curve.

is more commonly seen in adult TM patients with overt DM (17). In our study, the vast majority of pediatric TM patients showed pancreatic IO as measured by R2* relaxometry, and pancreatic fat infiltration was found in more than half of pediatric TM patients as measured by the IDEAL method. Notably, 17.8% of patients in our study had elevated fasting glucose levels, 80% of patients showed impaired insulin secretion capacity (HOMA-β), and 40% of patients showed decreased insulin sensitivity (HOMA-IR). The patients in our study were much younger than those reported by previous studies on pancreatic IO and fat infiltration (16,17,20). These findings emphasize the clinical relevancy of early monitoring of pancreatic IO in TM patients.

In our study, a homogenous distribution pattern of siderosis in the 3 pancreatic regions was seen when the iron deposition was mild to moderate. However, in cases of severe iron deposition, the distribution tends to be heterogeneous. These findings might be associated with pathologically progressive hemosiderin deposition processes from the initial deposition in the pancreatic exocrine tissue to selective deposition in the endocrine tissue (the islets) as IO increases, which has been verified by an autopsy study (18). Histologically, the exocrine tissue of the pancreas is homogeneously distributed among the pancreatic head, body, and tail, while the islets are heterogeneously scattered among the exocrine tissue (32,33). Fatty replacement was correlated with IO in pediatric TM patients in our study, which can also be found in adult TM patients (16). It is hypothesized that fatty replacement of the pancreas parenchyma follows iron deposition (18,19). However, our results showed that FF values in the tail region of the pancreas were higher than those in the head or body. A similar finding has also been reported in adult patients with IO disease, although not significant (16). Fatty replacement in the pancreas is supposed to represent the end or severe stage of pancreatic disease (34). It is known that more islets are present in the pancreatic tail compared with the head and body regions histologically (32,33). Therefore, it is not surprising that more fat content was found in the tail region as IO progressed.

In our study, pancreatic IO and fatty infiltration were more severe in patients with impaired glucose function than patients with normoglycemia. In adult TM patients, pancreatic iron deposition and fatty replacement have previously been shown to predict diabetes (2). In a recent study, pancreatic fatty replacement was also a predictor of diabetes in adult patients who had IO resulting from various hematological disorders, including TM (35). However, there is little existing data on the association between pancreatic IO, fat infiltration, and glucose metabolism in pediatric TM patients. Only İdilman *et al.* (20) have reported 3 teenage TM patients with elevated FF levels in the pancreas, however, the relationship between pancreatic fat infiltration and glycometabolism was not determined in their study. In our study, both iron accumulation and fatty replacement of the pancreas were associated with glucose dysregulation in TM children. Notably, fatty replacement of the pancreas in adult TM patients is irreversible with intensive chelation, and most likely represents the end or severe stage of pancreatic disease (34). Such irreversible damage to the pancreas might result from the cumulative destruction of beta cells (36). In our study, both pancreatic R2* relaxometry and FF were able to discriminate between pediatric TM patients with IFG and those with normoglycemia. Pancreatic FF showed a better discriminative power compared to R2* relaxometry, with an AUC of 0.931. These results suggest that regular measurement of pancreatic FF is also essential for the

management of children with TM, and pancreatic R2* relaxometry and FF can be used as potential risk factors for predicting the development of diabetes in pediatric TM patients.

Our study had several limitations. First, the patients were enrolled from 1 center, and the sample size was relatively small. Second, in our study, pancreatic iron was measured at 1.5T using the R2* acquisition technique, and FF was measured at 3.0T using the IDEAL algorithm. Since the co-occurrence of fat and iron in a voxel can confound each other (37), simultaneous measurement of R2* and FF using the T2*-IDEAL method would be more preferable if iron deposition is not severe (37,38). It has been shown that R2* provides precise iron quantification for lower IO at 3T, but does not work well for higher IO because susceptibility artifacts increase with field strength and signals can decay rapidly (39). In our study, we found that 11.1% (10/90) of patients had severe pancreatic IO. Thus, we used the widely accepted R2* acquisition technique equipped in our 1.5T scanner to measure iron in the pancreas (3,12,15). Fat suppression via CHESS in our study was used to minimize the effect of fat on T2* measurements. Due to the use of fat suppression, signal oscillation produced by fat, as described by Meloni *et al.* (40), was not obvious in our study. A fitting error <5% using CMRtools in our study also indicated good fitting quality. However, fat suppression via CHESS at 1.5T may lead to a systematic R2* reduction, especially for high R2* values (>900 s^{-1}) (41), though no patients in our study had an R2* value >900 s^{-1}. Third, the last TE of approximately 15 ms would be not adequate for precise R2* measurements in patients with no or moderate pancreatic IO at 1.5T. Last, no histological confirmation was performed for iron and fat content measurements by MRI. Although biopsy is the standard method for quantitative assessment of iron and fat in the pancreas, it has risks of procedure-related complications, sampling error, and interobserver variability (42,43). Moreover, it is not recommended for pediatric TM patients to receive a biopsy to evaluate the iron and fat content of the pancreas.

In conclusion, our study showed that pancreatic iron and fat can be measured quantitatively by gradient-echo imaging. In pediatric TM patients, hemosiderin in the pancreas may show a trend from initial homogenous deposition in the pancreatic exocrine tissue to heterogeneous deposition in the endocrine tissue as IO progresses. The heterogeneous fatty replacement may occur in the pancreas with higher fat content in the tail region. Pancreatic fatty replacement is associated with iron accumulation in pediatric TM patients. Both pancreatic IO and fat infiltration, as measured by gradient-echo imaging, are associated with the risk of developing diabetes in pediatric TM patients.

Acknowledgments

Funding: Sun Yat-sen University Clinical Research 5010 Program (Grant No: 2013004); Guangdong Natural Science Foundation (Grant No: 2018A0303130099).

Footnote

Conflicts of Interest: All authors have completed the ICMJE uniform disclosure form (available at http://dx.doi.org/10.21037/qims-20-292). HG serves as an unpaid editorial board member of *Quantitative Imaging in Medicine and Surgery*. The other authors have no conflicts of interest to declare.

Ethical Statement: The institutional review board approved this prospective study of Sun Yat-sen Memorial Hospital of Sun Yat-sen University (No. 2013-19). Written informed consent was obtained from all patients or their parents.

References

1. Borgna-Pignatti C, Rugolotto S, De Stefano P, Zhao H, Cappellini MD, Del VG, Romeo MA, Forni GL, Gamberini MR, Ghilardi R, Piga A, Cnaan A. Survival and complications in patients with thalassemia major treated with transfusion and deferoxamine. Haematologica 2004;89:1187-93.
2. Au WY, Lam WWM, Chu W, Tam S, Wong WK, Liang R, Ha SY. A T2* magnetic resonance imaging study of pancreatic iron overload in thalassemia major. Haematologica 2008;93:116-9.
3. Noetzli LJ, Mittelman SD, Watanabe RM, Coates TD,

Wood JC. Pancreatic iron and glucose dysregulation in thalassemia major. Am J Hematol 2012;87:155-60.
4. Cario H, Holl RW, Debatin KM, Kohne E. Insulin sensitivity and beta-cell secretion in thalassaemia major with secondary haemochromatosis: assessment by oral glucose tolerance test. Eur J Pediatr 2003;162:139-46.
5. Li MJ, Peng SS, Lu M, Chang H, Yang Y, Jou S, Lin D, Lin K. Diabetes mellitus in patients with thalassemia major. Pediatr Blood Cancer 2014;61:20-4.
6. Pepe A, Meloni A, Rossi G, Caruso V, CUccia L, Spasiano A, Gerardi C, Zuccarelli A, D'Ascola DG, Grimaldi S, Santodirocco M, Campisi S, Lai ME, Piraino B, Chiodi E, Ascioti C, Gulino L, Positano V, Lombardi M, Gamberini MR. Cardiac complications and diabetes in thalassaemia major: a large historical multicentre study. Br J Haematol 2013;163:520-7.
7. De Sanctis V, Eleftheriou A, Malaventura C; Thalassaemia International Federation Study Group on Growth and Endocrine Complications in Thalassaemia. Prevalence of endocrine complications and short stature in patients with thalassaemia major: a multicenter study by the Thalassaemia International Federation (TIF). Pediatr Endocrinol 2004;Rev 2:249-55.
8. Brittenham GM, Griffith P, Nienhuis A, Mclaren CE, Young NS, Tucker EE, Allen CJ, Farrell DE, Harris JW. Efficacy of deferoxamine in preventing complications of iron overload in patients with thalassemia major. N Engl J Med 1994;331:567-73.
9. Noetzli LJ, Papudesi J, Coates TD, Wood JC. Pancreatic iron loading predicts cardiac iron loading in thalassemia major. Blood 2009;114:4021-6.
10. Meloni A, Restaino G, Missere M, De Marchi D, Positano V, Valeri G, D'Ascola DG, Peluso A, Putti MC, Lendini M, Neri MG, Midiri M, Sallustio G, Pepe A. Pancreatic iron overload by T2* MRI in a large cohort of well treated thalassemia major patients: can it tell us heart iron distribution and function? Am J Hematol 2015;90:E189-90.
11. Wood JC. Estimating tissue iron burden: current status and future prospects. Br J Haematol 2015;170:15-28.
12. Wood JC, Enriquez C, Ghugre N, Michael Tyzka J, Carson S, Nelson MD, Coates TD. MRI R2 and R2* mapping accurately estimates hepatic iron concentration in transfusion-dependent thalassemia and sickle cell disease patients. Blood 2005;106:1460-5.
13. St Pierre TG, Clark PR, Chua-anusorn W, Fleming,AJ, Jeffrey GP, Olynyk JK, Pootrakul P, Robins E, Lindeman R. Noninvasive measurement and imaging of liver iron concentrations using proton magnetic resonance. Blood 2005;105:855-61.
14. Wood JC, Tyszka JM, Carson S, Nelson MD, Coates TD. Myocardial iron loading in transfusion-dependent thalassemia and sickle cell disease. Blood 2004;103:1934-6.
15. Anderson LJ, Holden S, Davis B, Prescott E, Charrier CC, Bunce NH, Firmin DN, Wonke B, Porter J, Walker JM, Pennell DJ. Cardiovascular T2-star (T2*) magnetic resonance for the early diagnosis of myocardial iron overload. Eur Heart J 2001;22:2171-9.
16. Pfeifer CD, Schoennagel BP, Grosse R, Wang ZJ, Graessner J, Nielsen P, Adam G, Fischer R, Yamamura J. Pancreatic iron and fat assessment by MRI-R2* in patients with iron overload diseases. J Magn Reson Imaging 2015;42:196-203.
17. Papakonstantinou O, Ladis V, Kostaridou S, Maris T, Berdousi H, Kattamis C, Gourtsoyiannis N. The pancreas in β-thalassemia major: MR imaging features and correlation with iron stores and glucose disturbunces. Eur Radiol 2007;17:1535-43.
18. Lu JP, Hayashi K. Selective iron deposition in pancreatic islet B cells of transfusional iron-overloaded autopsy cases. Pathol Int 1994; 44:194-9.
19. Kim KH, Kim CD, Ryu HS, Hyun JH, Chung JP, Chung JB, Kang KJ, Chi HS, Park JJ. Endoscopic retrograde pancreatographic findings of pancreatic lipomatosis. J Korean Med Sci 1999;14:578-81.
20. İdilman İS, Gümrük F, Haliloğlu M, Karçaaltıncaba M. The Feasibility of Magnetic Resonance Imaging for Quantification of Liver, Pancreas, Spleen, Vertebral Bone Marrow, and Renal Cortex R2* and Proton Density Fat Fraction in Transfusion-Related Iron Overload. Turk J Haematol 2016;33:21-7.
21. Cole TJ, Bellizzi MC, Flegal KM, Dietz WH. Establishing a standard definition for child overweight and obesity worldwide: international survey. BMJ 2000;320:1240-3.
22. He T, Gatehouse PD, Smith GC, Mohiaddin RH, Pennell DJ, Firmin DN. Myocardial T2* measurements in iron-overloaded thalassemia: An in vivo study to investigate optimal methods of quantification. Magn Reson Med 2008;60:1082-9.
23. Reeder SB, McKenzie CA, Pineda AR, Yu H, Shimakawa A, Brau AC, Hargreaves BA, Gold GE, Brittain JH. Water-fat separation with IDEAL gradient-echo imaging. J Magn Reson Imaging 2007;25:644-52.
24. Wahidiyat PA, Iskandar SD, Sekarsari D. Evaluation of iron overload between age groups using magnetic resonance imaging and its correlation with iron profile in transfusion-dependent thalassemia. Acta Med Indones

2018;50:230-6.
25. Sijens PE, Edens MA, Bakker SJ, Stolk RP. MRI-determined fat content of human liver, pancreas and kidney. World J Gastroenterol 2010; 16:1993-8.
26. American Diabetes Association. Classification and diagnosis of diabetes. Diabetes Care 2015;38:S8-16.
27. Berdoukas V, Nord A, Carson S, Puliyel M, Hofstra T, Wood J, Coates TD. Tissue iron evaluation in chronically transfused children shows significant levels of iron loading at a very young age. Am J Hematol 2013;88:E283-5.
28. Piperno A. Classification and diagnosis of iron overload. Haematologica 1998;83:447-55.
29. Vasanawala SS, Yu H, Shimakawa A, Jeng M, Brittain JH. Estimation of liver T_2 in transfusion-related iron overload in patients with weighted least squares T_2 IDEAL. Magn Reson Med 2012;67:183-90.
30. Chen Y, Jiang Z, Long L, Miu Y, Zhang L, Zhong D, Tang Q. Magnetic resonance imaging: Proton density fat fraction for assessment of pancreatic fatty infiltration during progression of T2DM bama minipigs. J Magn Reson Imaging 2019;50:1905-13.
31. Hu F, Yang R, Huang Z, Wang M, Yuan F, Xia C, Wei Y, Song B. 3D Multi-Echo Dixon technique for simultaneous assessment of liver steatosis and iron overload in patients with chronic liver diseases: a feasibility study. Quant Imaging Med Surg 2019;9:1014-24.
32. Wittingen J, Frey CF. Islet concentration in the head, body, tail and uncinate process of the pancreas. Ann Surg 1974;179:412-4.
33. Longnecker D. Anatomy and Histology of the Pancreas. The pancreapedia: Exocrine Pancreas Knowledge Base. Available online: http://dx.doi.org/10.3998/panc.2014.3, Accessed 2014.
34. Midiri M, Lo Casto A, Sparacia G, D'Angelo P, Malizia R, Finazzo M, Montalto G, Solbiati L, Lagalla R, De Maria M. MR imaging of pancreatic changes in patients with transfusion-dependent beta-thalassemia major. AJR Am J Roentgenol 1999;173:187-92.
35. Shur J, Kannengiesser SAR, Menezes R, Ward R, Kuo K, Jhaveri K. Glucose dysregulation in patients with iron overload: is there a relationship with quantitative pancreas and liver iron and fat content measured by MRI? Eur Radiol 2020;30:1616-23.
36. Messina MF, Lombardo F, Meo A, Miceli M, Wasniewska M, Valenzise M, Ruggeri C, Arrigo T, De Luca F. Three-year prospective evaluation of glucose tolerance, beta-cell function and peripheral insulin sensitivity in non-diabetic patients with thalassemia major. J Endocrinol Invest 2002;25:497-501.
37. Yu H, McKenzie CA, Shimakawa A, Vu AT, Brau ACS, Beatty PJ, Pineda AR, Brittain JH, Reeder SB. Multiecho reconstruction for simultaneous water-fat decomposition and T2* estimation. J Magn Reson Imaging 2007;26:1153-61.
38. Hernando D, Levin YS, Sirlin CB, Reeder SB. Quantification of liver iron with MRI: state of the art and remaining challenges. J Magn Reson Imaging 2014;40:1003-21.
39. d'Assignies G, Paisant A, Bardou-Jacquet E, Boulic A, Bannier E, Lainé F, Ropert M, Morcet J, Saint-Jalmes H, Gandon Y. Non-invasive measurement of liver iron concentration using 3-Tesla magnetic resonance imaging: validation against biopsy. Eur Radiol 2018;28:2022-30.
40. Meloni A, De Marchi D, Positano V, Neri MG, Mangione M, Keilberg P, Lendini M, Cirotto C, Pepe A. Accurate estimate of pancreatic T2* values: how to deal with fat infiltration. Abdom Imaging 2015;40:3129-36.
41. Krafft AJ, Loeffler RB, Song R, Bian X, McCarville MB, Hankins JS, Hillenbrand CM. Does fat suppression via chemically selective saturation affect R2*-MRI for transfusional iron overload assessment? A clinical evaluation at 1.5T and 3T. Magn Reson Med 2016;76:591-601.
42. Standish RA, Cholongitas E, Dhillon A, Burroughs AK, Dhillon AP. An appraisal of the histopathological assessment of liver fibrosis. Gut 2006;55:569-78.
43. Bravo AA, Sheth SG, Chopra S. Liver biopsy. N Engl J Med 2001;344:495-500.

Cite this article as: Huang J, Shen J, Yang Q, Cheng Z, Chen X, Yu T, Zhong J, Su Y, Guo H, Liang B. Quantification of pancreatic iron overload and fat infiltration and their correlation with glucose disturbance in pediatric thalassemia major patients. Quant Imaging Med Surg 2021;11(2):665-675. doi: 10.21037/qims-20-292

